Assiut University Journal of Multidisciplinary Scientific Research (AUNJMSR)
Faculty of Science, Assiut University, Assiut, Egypt.
Printed ISSN 2812-5029
Online ISSN 2812-5037
Vol. 54(1): 44- 64 (2025)
https://aunj.journals.ekb.eg

Geophysical investigation of probable interconnection between the deep and shallow aquifers in the western bank of the Nile River from Aswan to Sohag governorates, Upper Egypt

Ibrahim A. Ibrahim[1,*], Abotalib Z. Abotalib[2,3], Haby S. Mohamed[1], Mahmoud M. Senosy[1]

[1]Geology Department, Faculty of Science, Assiut University, Assiut, Egypt

[2]Division of Geological Applications and Mineral Resources, National Authority for Remote Sensing and Space Sciences, Cairo, Egypt

[3]National Center for Environmental Compliance, Riyadh, Saudi Arabia

[*]Corresponding Author: ibrahimaboasem@science.aun.edu.eg

ARTICLE INFO

Article History:
Received: 2024-07-28
Accepted: 2024-10-20
Online: 2024-12-26

Keywords:
Groundwater aquifers, Nubian Sandstone Aquifer System (NSAS), Quaternary Aquifer System (QAS), aeromagnetic data analysis.

ABSTRACT

Aeromagnetic data was analyzed to reveal the subsurface deep-seated major faults whereas major surface faults were traced from the published geological maps of Egypt. The analysis and interpretation of these data, in combination with surface faults, revealed that the main prevailing structural trends run in an E-W, NW-SE and NE-SW directions for deep and surface faults, respectively. It was inferred that these faults are of regional aspect and extend from the deep subsurface to the shallow surface. The continuity between the deep-seated and the surface faults may forecast a possible vertical connection between the deep Nubian Sandstone Aquifer System (NSAS) and the Quaternary Aquifer System (QAS). This suggestion is supported by previously published isotopic

analyses in the region.

1. INTRODUCTION

Groundwater resources assessment in Egypt is essential due to the water scarcity we are facing nowadays in our hyper-arid region. The recharge process from deep mega towards shallow aquifers is a significant issue. Such recharge, for instance via vertical and sub-vertical faults, can feed easily accessible, highly consumable, shallow aquifers. Geophysical investigation plays therefore an important role in the process of groundwater evaluation by addressing groundwater potentiality; providing spatially extensive, non-invasive means of investigating the subsurface [1]. Among the various geophysical techniques, magnetic methods stand out for their ability to detect the subsurface structures and faults [3].

Deep and shallow aquifers interconnection is a known worldwide phenomenon such as the High Plains Aquifer, USA, which demonstrates a significant vertical connection between shallow and deep water zones [9]. Understanding the hydrogeological connection between aquifers is necessary for the purposes of sustainable water resource management, particularly in areas facing water scarcity. The hydrogeological connection between different aquifers involves the movement of water across subsurface reservoirs, driven by geological, hydrological, and man-induced factors [4, 5]. Subsurface structures (e.g. faults) significantly impact the vertical connectivity between aquifers [6]. Understanding how faults influence vertical groundwater flow is essential for effective groundwater management, particularly in regions with complex geology and multiple aquifer systems [7]. The hydrogeological interconnection can be achieved vertically and sub-vertically throughout faults and fractures, allowing water to cross confining layers and move vertically between aquifers. The pathways can significantly enhance the vertical connectivity, particularly in areas with significant tectonic activity [8].

The current study area lies between longitudes 30° to 33° E and latitudes 24.25° to 26.5° N (figure 1), including the western bank of the Nile River. It aims to predict the connection status between the deep Nubian Sandstone Aquifer System (NSAS) and the

shallow Quaternary Aquifer System (QAS) in the study area from Aswan to Sohag governorates. This investigation is accomplished through analyzing aeromagnetic data prepared by the Egyptian General Petroleum Corporation in 1989 (scale 1:500,000). The

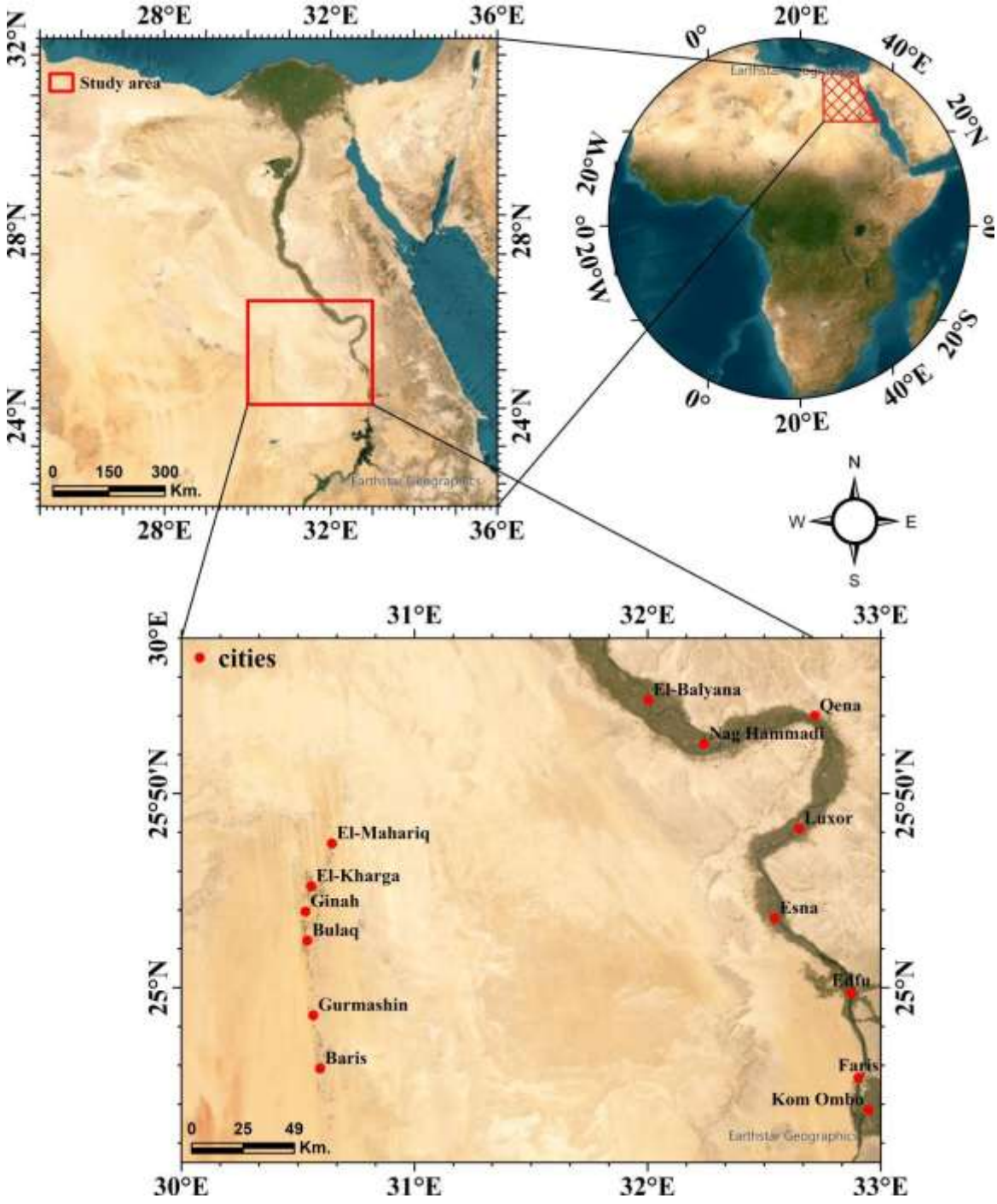

Fig. 1: Satellite imagery map show, A) The location of Africa, B) The location of Egypt, C) The location map of the study

major surface faults are traced from the geological map of Egypt (scale 1:2,000,000) published by the Egypt Geological Survey and Mining Authority in 1981. The deep subsurface faults are correlated to the surface faults to examine their attitudes and the degree of continuity.

2. GEOLOGICAL/HYDROGEOLOGICAL SETTING

The general geology of the study area (Fig. 2) is discussed by [10]. The sedimentary succession of the southern part of Egypt in general, including the study area, was deposited in the form of two huge sedimentary basins, the Dakhla Basin in the west and the Assiut Basin in the east [11]. The sedimentary rocks that adjoin the Nile Valley were formed during Mesozoic and Cenozoic and were classified into two main facies: Berriasian-Campanian and Campanian-Lower Eocene. Nubia Group units, namely Six Hills, Abu Ballas, Sabaya, Maghrabi, and Taref formations, from older to younger, respectively are known. Three of them are chunky of predominant fluviatile origin; the Six Hills, Sabaya and Taref formations. The remaining two units are thin, partly marginal marine clastic units: the Abu Ballas and Maghrabi formations, intercalating the previous units, [12, 13]. The Nubia Group and the overlying Quseir Formation sedimentation ended during the Santonian, when the marine conditions dominated (i.e. the Campanian-Ypresian transgression peak) [13]. The Campanian-lower Ypresian is a shallow-marine succession represented by the Quseir, Duwi, Dakhla, Tarawan, and Esna formations. This succession is followed conformably by the latest Ypresian predominantly carbonate succession, known as the Thebes Formation [14]. The quaternary sediments in the study area are represented by The Armant, Idfu and Qena formations. These formations are composed of alternating beds of conglomerate, varied-size sands, and clay beds [15].

The NSAS is one of the largest and oldest groundwater reservoirs in the world that covers over 2 million square kilometers. It extends beneath four countries in North Africa: Egypt, Libya, Sudan, and Chad [16]. This aquifer is composed of sandstones of Paleozoic to Cretaceous ages. In Egypt, it lies primarily beneath the Eastern Sahara, extending It is characterized by high porosity and permeability, which facilitates significant groundwater storage and flow [16]. The QAS in Egypt is a significant groundwater resource, primarily situated in the Nile Valley and Nile Delta regions. It

plays a crucial role in supporting agriculture, industry, and other domestic uses. It is composed of unconsolidated sands, gravels, silts, and clays of Quaternary ages [17]. These sediments were deposited by the Nile River and its tributaries over thousands of years, creating a highly variable and heterogeneous aquifer system [18].

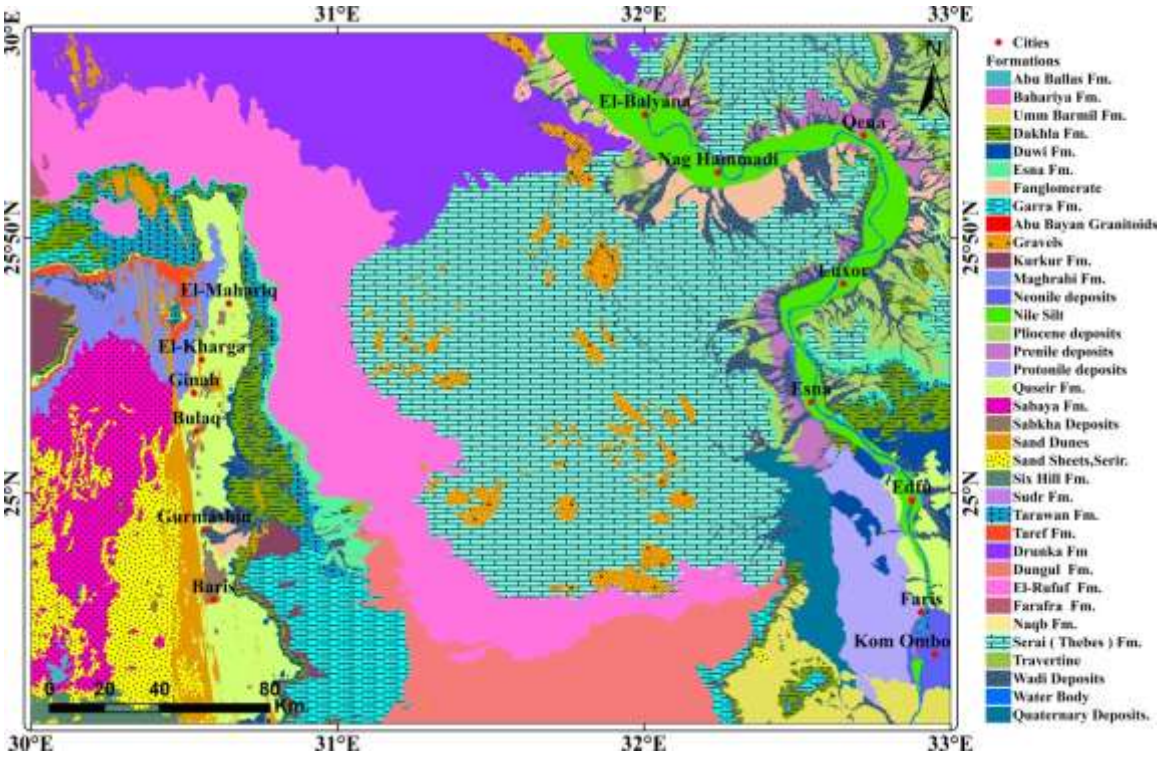

Fig. 2: Geologic map of the study area, modified after [10].

3. MATERIALS AND METHODS

The used data are (1) aeromagnetic maps with a scale of 1: 500,000 released in 1989 by the Egyptian General Petroleum Company with a contour interval of 25 nT. (2) geologic maps compiled from [10] to represent the geological formations distributed in the study area. (3) The geologic map of Egypt by the Egyptian Geological Survey and Minning Authority [19] to trace the major surface faults in the study area. The main processing software is Geosoft Oasis Montaj v8.4. to grid and process the aeromagnetic data [20].

3.1. Upward continuation:

The upward continuation technique is particularly useful in distinguishing between shallow and deep magnetic sources by smoothing out near-surface anomalies and emphasizing deeper sources, thus aiding in subsurface exploration [22]. Mathematically, it involves solving the Laplace equation, which describes the potential field, and extending the magnetic data from a lower to a higher plane [23]. The process involves Fourier transformation, allowing the separation of high-frequency components (near-surface anomalies) from low-frequency components (deeper sources). The mathematical expression in the wavenumber domain of this filter is given by equation (1) as follows:

$$\mathbf{L(k) = e^{-2\pi hk}} \quad (\mathbf{1})$$

Where, k is the wavenumber domain increment, used to depict a radially symmetrical variable and h is the distance in ground units, relative to the plane of observation to continue upward.

3.2. First Vertical Derivative (FVD):

The vertical derivatives are used clearly to realize the situation at very shallow depths and bring out the hidden local variation in the potential field data that could not be detected by the regional–residual separations, as well as to improve the clearance of geological contacts [23]. The First Vertical Derivative (FVD) is given via the formula (2) as follows:

$$\mathbf{FVD = \frac{dT}{dz}} \quad (\mathbf{2})$$

Where T is the total magnetic field.

3.3. Butterworth high pass filter:

This filter is designed to remove low-frequency components of the signal, thus emphasizing higher-frequency anomalies associated with near-surface geological features. This filter provides a smooth and efficient way to emphasize higher-frequency components while suppressing unwanted low-frequency noise [24]. Equation (3) shows the mathematical formula of this filter.

$$\mathbf{L(k) = \frac{\frac{k}{k_c}}{\left[1+\left(\frac{k}{k_c}\right)^n\right]}} \quad (\mathbf{3})$$

Where, k is the wavenumber domain increment, k_c is the Inflection point of wavenumber cutoff in cycles/ ground unit and n is a positive integer value determining the degree of sharpness of the cutoff

3.4. Analytic Signal (AS):

The analytic signal filter (AS) is calculated as the square root of the sum of the squares of the vertical and the two horizontal derivatives of the total field. The analytic signal is useful in locating the edges of magnetic source bodies. The analytical signal approach has been successively used in the form of 3D interpretation of aeromagnetic data [25]. Equation (4) displays the mathematical formula for the AS as follows:

$$\mathbf{AS} = \sqrt{\left(\frac{\mathbf{dT}}{\mathbf{dx}}\right)^{\mathbf{2}} + \left(\frac{\mathbf{dT}}{\mathbf{dy}}\right)^{\mathbf{2}} + \left(\frac{\mathbf{dT}}{\mathbf{dz}}\right)^{\mathbf{2}}} \quad (\mathbf{4})$$

Where $\left(\frac{dT}{dx}\right), \left(\frac{dT}{dy}\right), \left(\frac{dT}{dz}\right)$ are the first order derivatives of the magnetic field in the x, y and z directions respectively.

3.5. Tilt Derivative:

The tilt derivative filter is obtained from the first vertical derivative of the field by dividing it by the total horizontal derivative of the field in the X and Y directions. The zero contours of the tilt angle match the contacts of geologic abrupt discontinuities and are used to delineate the linear anomalies in potential field data. It is a commonly used filter as it has a powerful job of mapping shallow subsurface structures, without the noise amplification that can occur in higher-order vertical derivative grids [26]. The mathematical formula for this filter is expressed in equation (5):

$$\boldsymbol{TDR} = \frac{\boldsymbol{FVD}}{\boldsymbol{THD}} \quad (\mathbf{5})$$

where FVD is the first vertical derivative (Eq. 2) and THD is the total horizontal gradient of the magnetic field (Eq. 6):

$$\boldsymbol{THD} = \sqrt{\left(\frac{\boldsymbol{dT}}{\boldsymbol{dx}}\right)^{\mathbf{2}} + \left(\frac{\boldsymbol{dT}}{\boldsymbol{dy}}\right)^{\mathbf{2}}} \quad (\mathbf{6})$$

4. RESULTS AND DISCUSSION

4.1. RTP map

The RTP map (fig. 3A) shows that the intensity of the magnetic bodies ranges from -185 to 151 nT. The high-magnitude magnetic bodies are scattered in the southern part more than in the northern part. This distribution reflects that the basement rocks in the

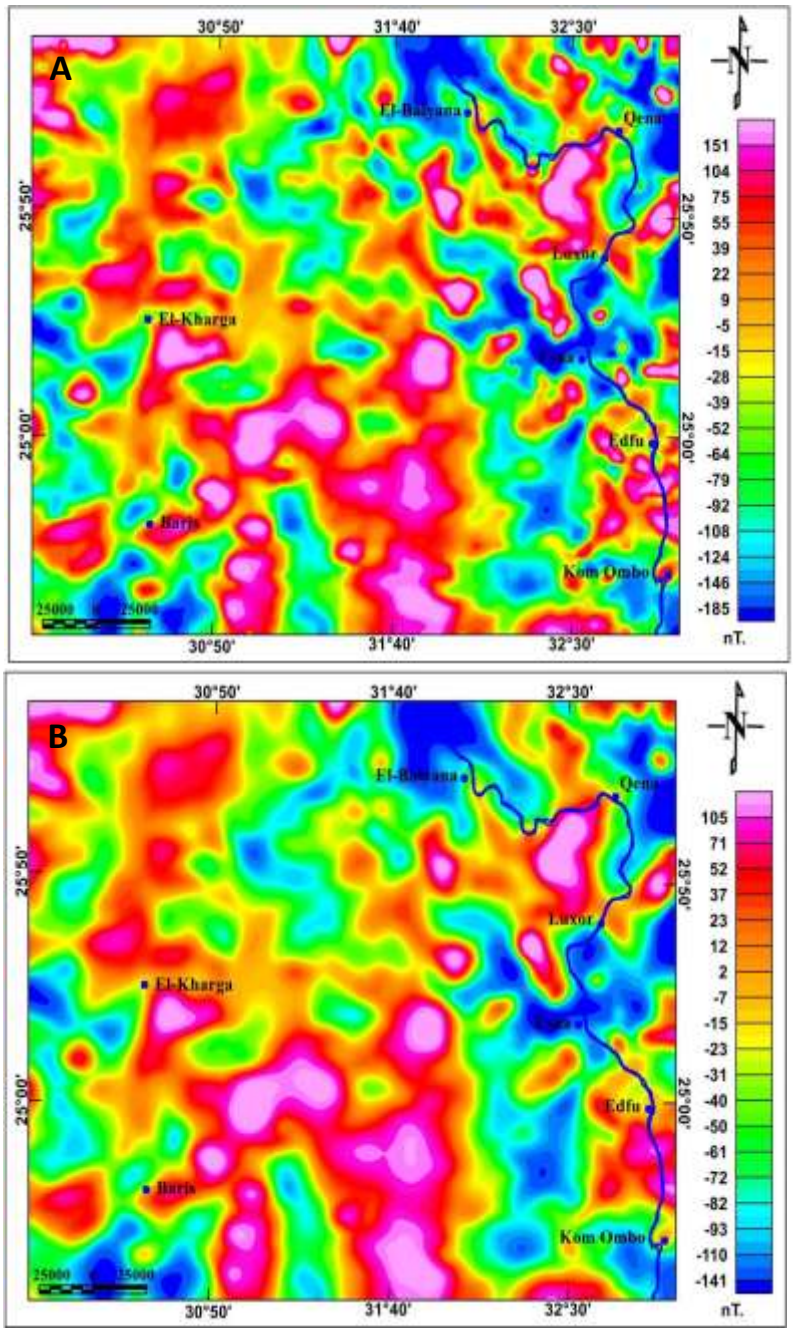

Fig. 3: (A) RTP map of the study area, (B) Upwardly continued map of the RTP map by 3000 meters.

southern part of the study area are shallower than in the north and, consequently, manifests a more northward thick sedimentary cover.

4.2. Upward continuation map:

Figure (3B) shows the upward continuation map of the RTP map of the study area, the upward continuation filter was applied by a distance of 3000 to minimize the effects of shallow sources and noise. The resulting map has smooth anomalies rather than the RTP and this has led to a smooth processing and filtration operation, appropriate for regional structural mapping in this area. The higher magnetic anomalies are located in the middle south, the far eastern south, the eastern north, and the western north parts. These bodies have a magnitude ranging from 37 to 105 nT. The lowest anomalies are located in the southeastern corner, the middle east, and middle northern parts of the map. These bodies have magnitudes from -141 to -93 nT. The high bodies imply a shallower basement rocks.

4.3. First vertical derivative:

The first vertical derivative map (Fig. 4A) reveals the faults across the study area where the zero contour line denotes a structural boundary between high and low magnetic anomalies. It represents the edges between magnetic bodies and consequently reflects fault lines (Fig. 4B). These faults are traced and analyzed as shown in figure 5. The dominant are the E-W and the NW-SE trends as revealed by the rose diagram.

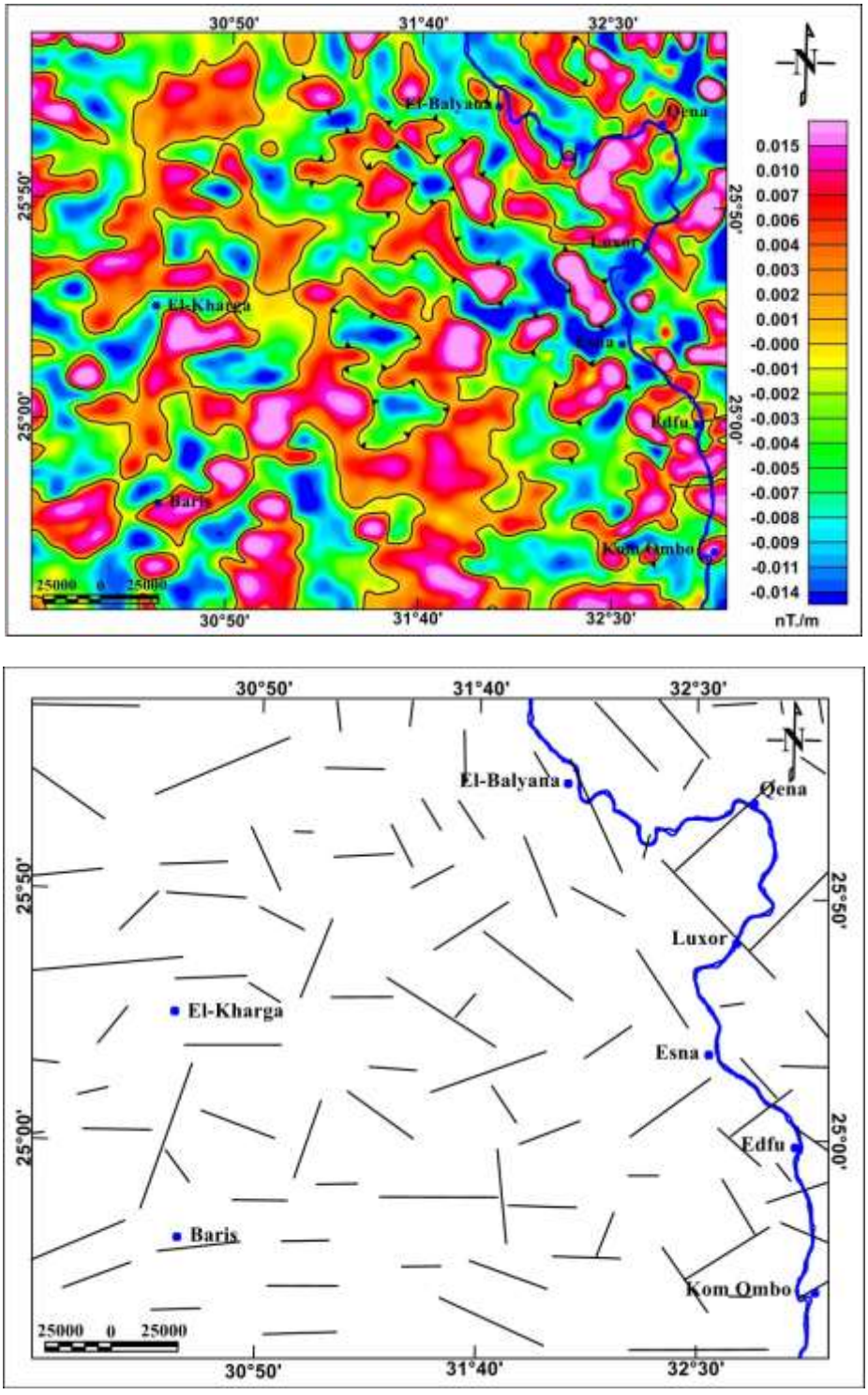

Fig. 4: (A) The first vertical derivative (FVD) map, (B) Faults traced based on map 4A.

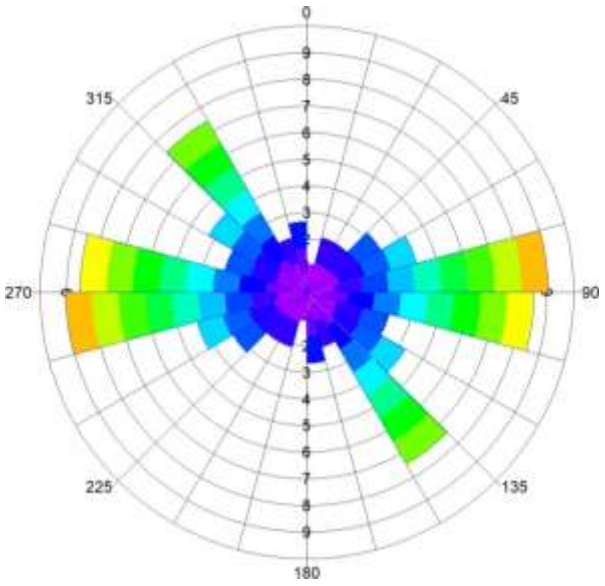

Fig. 5: Rose diagrams for the fault trends for First vertical derivative (FVD) filter

4.4. Butterworth high pass filter:

Figure (6A) represents the Butterworth high pass filter that depicts the subsurface in a smoother pattern than the FVD. From this map it be seen that the main trends of the subsurface faults (Fig. 6B) are the E-W trend with minor NW-SE, and NE-SW trends (Fig. 7).

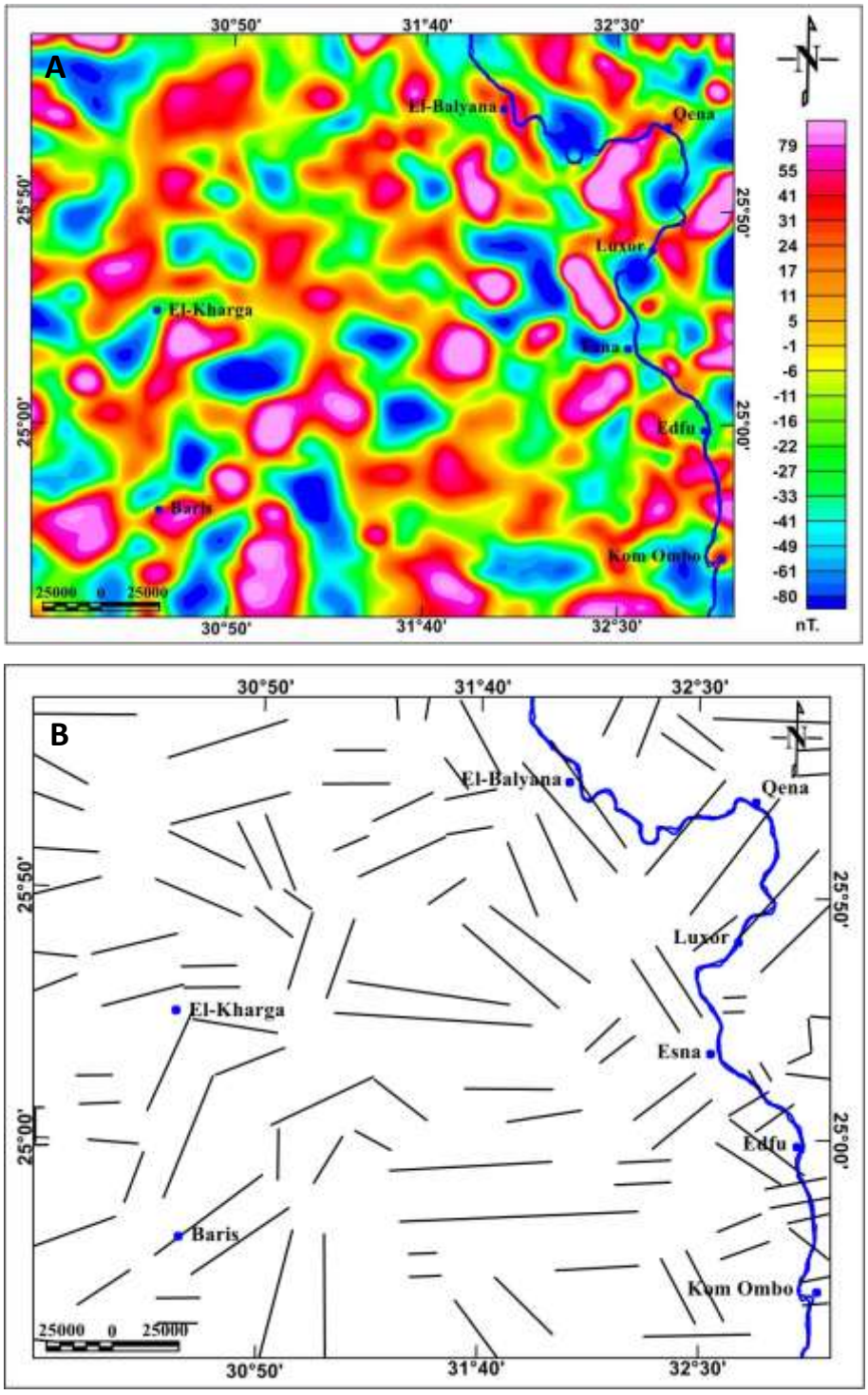

Fig. 6: (A) Butterworth High pass map of the study area, (B) Faults traced based on map 6A.

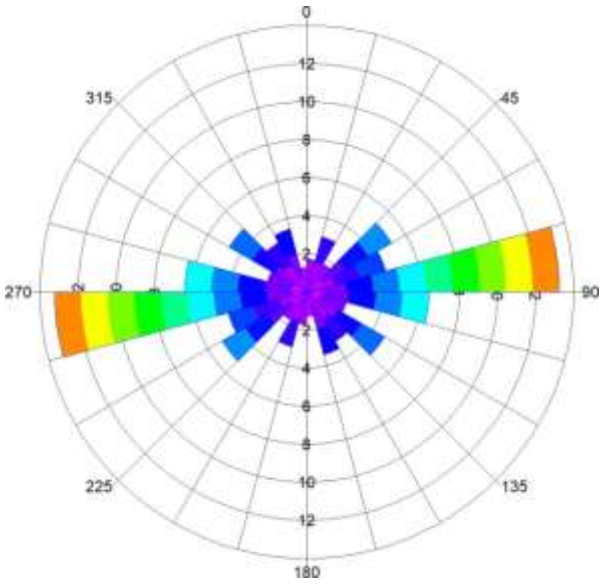

Fig. 7: Rose diagrams for the fault trends for Butterworth high pass filter.

4.5. Tilt derivative filter:

The maxima values of the tilt derivative filter (Fig. 8) represent the major subsurface faults. These values in the tilt derivative map were mapped and the zero contour line (Fig. 8B), represents the edge of the magnetic bodies and/or the contacts between different rocks. Such contacts and edges are coincident fault lines. All fault lines were traced and presented on a rose diagram (Fig. 9). This diagram shows the faults trends as appearing on figure 9, which shows an E-W, NW-SE, and NE-SW, respectively.

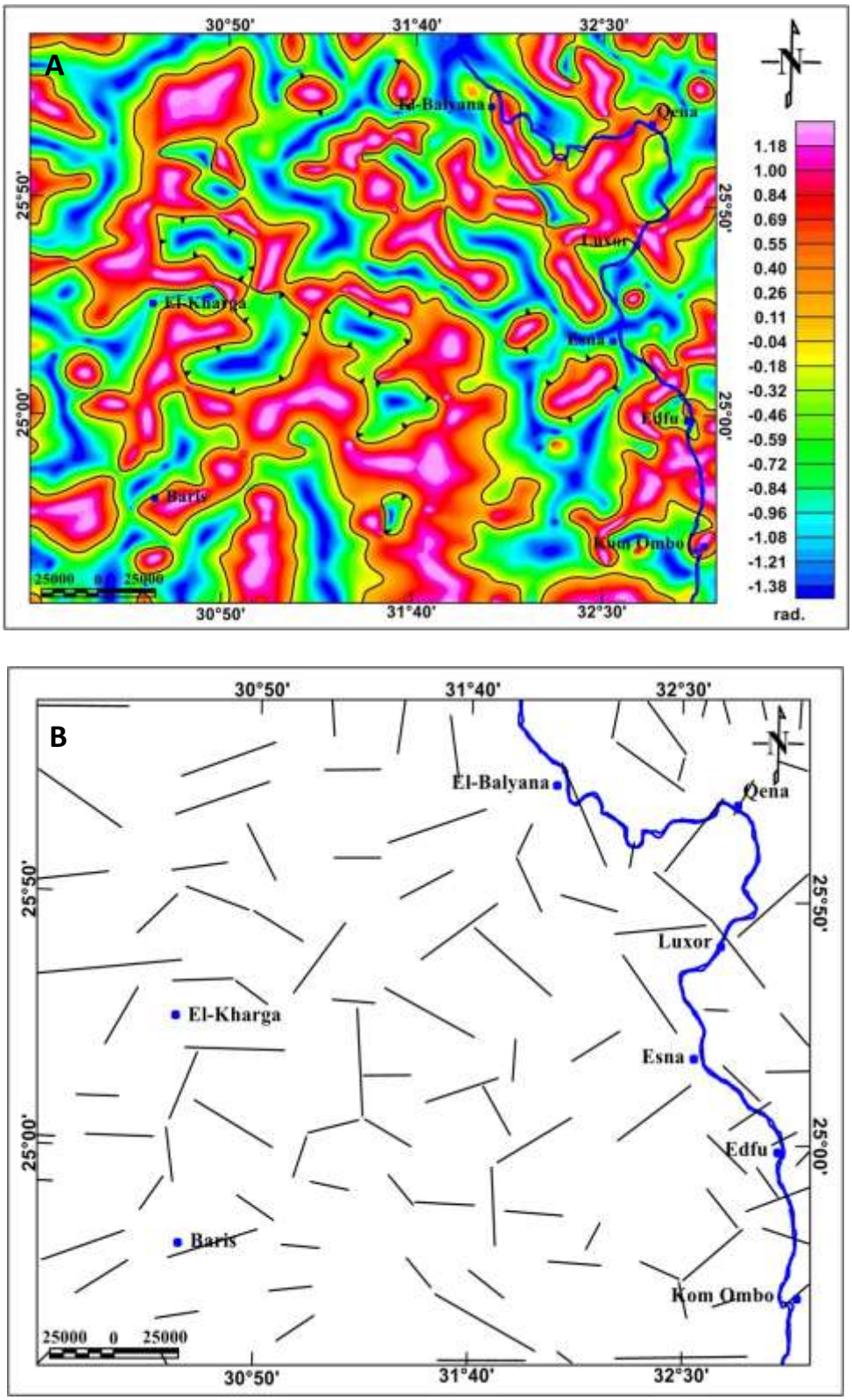

Fig. 8: (A) Tilt derivative filter map, (B) faults traced based on map 8A.

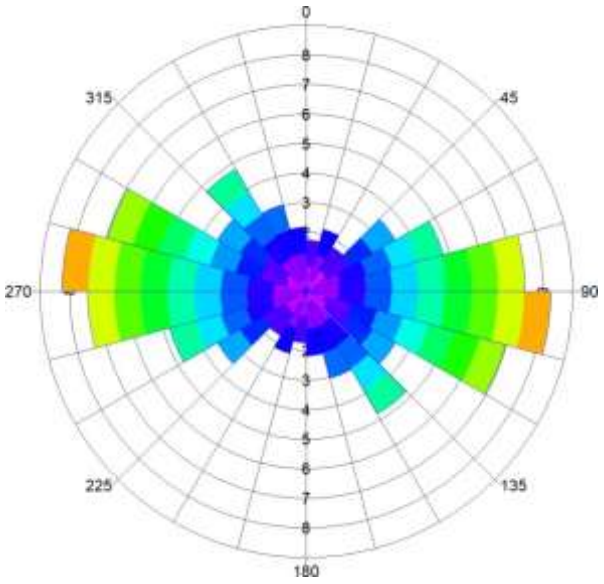

Fig. 9: Rose diagrams for the fault trends Tilt derivative filter.

4.6. Analytical Signal filter:

Analytical signal has the main advantage of delineating concealed magnetic bodies and enhancing their edges. Figure (10A) displays the obtained analytical signal filter map where the high magnitudes are characteristic of the bodies that are high in their magnetic properties. These magnetic bodies delineate the concealed subsurface faults (Fig. 10B). Figure (11) is the rose diagram with the trends analyzed from the analytical signal filter. The main trend is the E-W with its subcomponents (NW-W and NE-E), and the NW-SE; the NE- SE is less dominant.

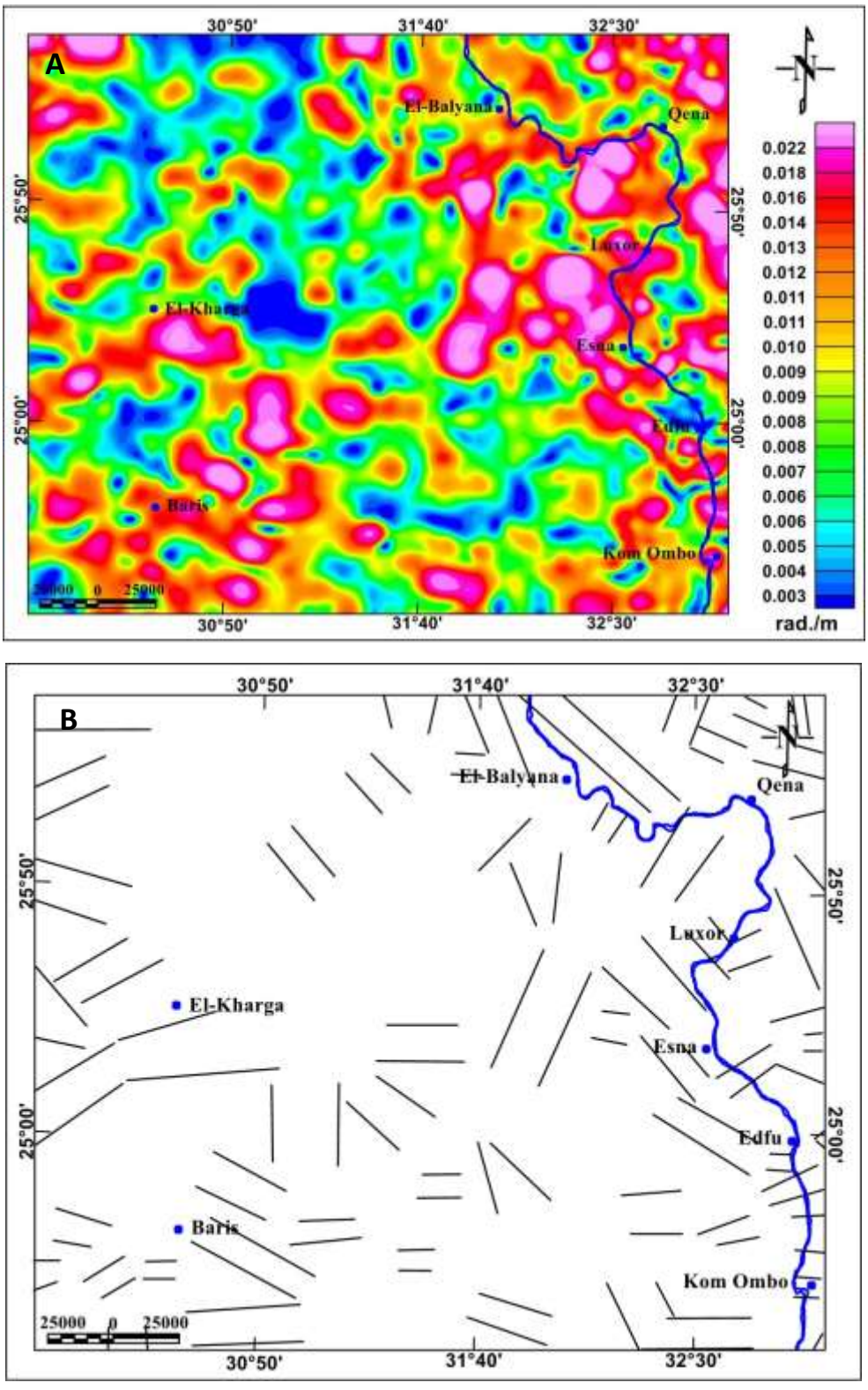

Fig.10: (A) Analytical signal map, (B) faults trends based on map 10A

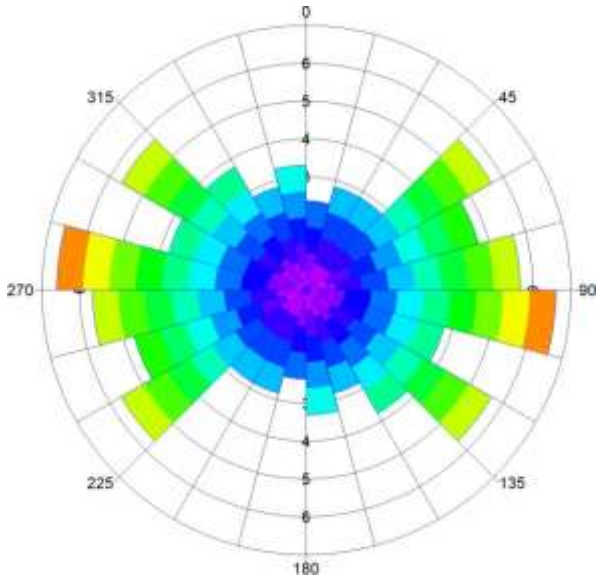

Fig. 11: Rose diagrams for the fault trends for Analytical signal filter

4.7. Surface faults:

The major surface faults in the study area are traced from the geological map of Egypt released by the Egyptian Geological Survey and Mining Authority in 1981[18] (Fig. 12A). The trends of these faults are illustrated by the rose diagram of figure (12B). Their main trends are E-W and N-S with a minor NW-SE trending.

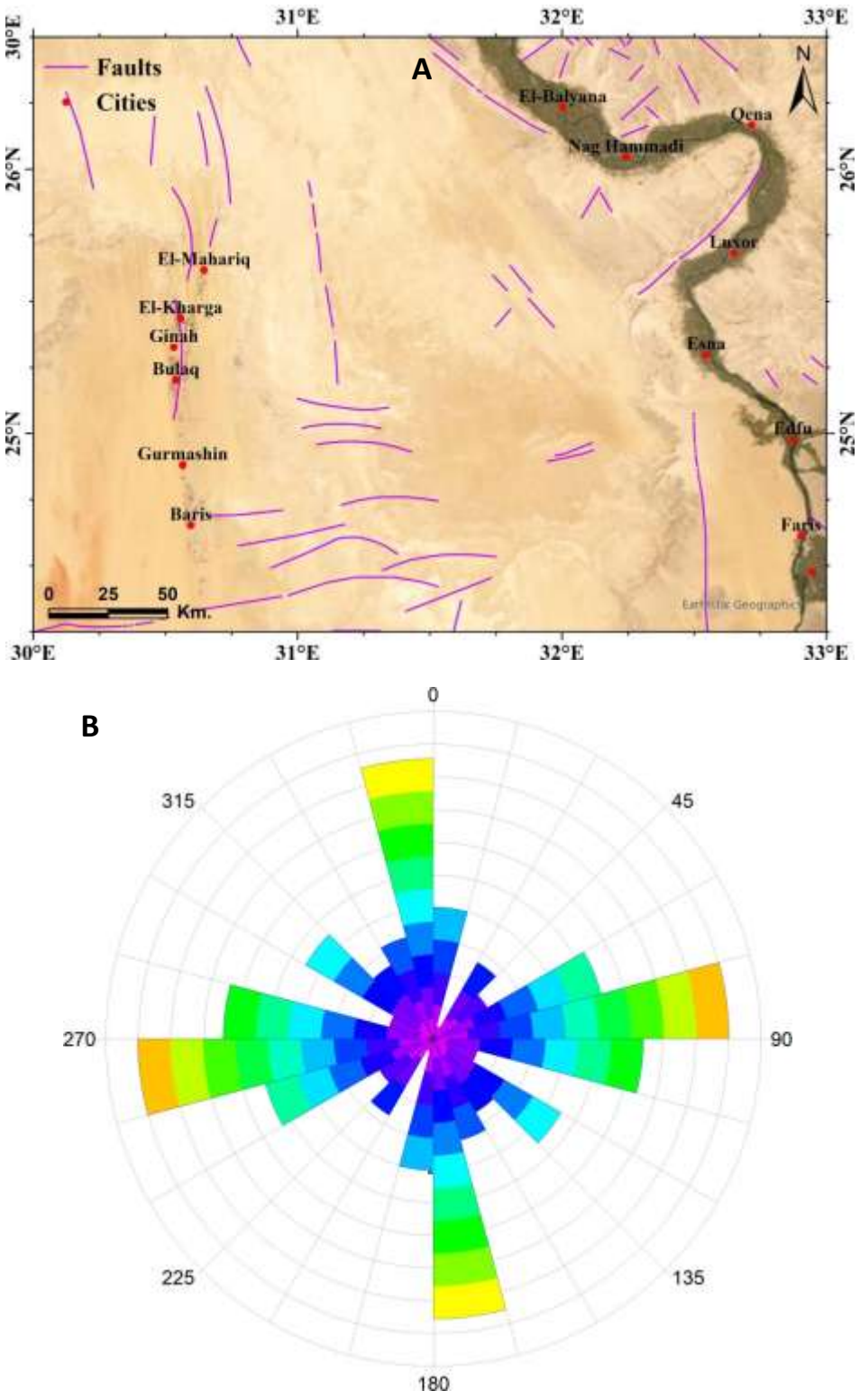

Fig. 12: (A) Surface faults traced from [18], (B) Rose diagram showing their trends.

5. CONCLUSION

The magnetic data and geologic maps seem to reveal the major subsurface and surface faults, respectively. Results of the applied filters show major fault trends in the E-W and NW-SE trends and the surface faults trending, more or less, comparable E-W, N-S trending. This implies a good correlation between the major surface and subsurface faults, especially the E-W trending. This correlation might indicate a continuity of the faults that may control the hydrogeological connection between the aquifer systems in the study area. This may explain a probable hydrogeological interconnection between the NSAS and the QAS and suggests, therefore, a possibility that the deep aquifer can feed the shallow one. This can be achieved through vertical and sub-vertical faults and structures. Our hypothesis is supported from the structural perspective of [27], where they interpreted seismic sections as reflecting the fault continuity in Komombo Basin. Another supporting evidences can be seen from the hydrogeological achievements of [28] and from the isotopic composition of the groundwater samples in the study area at Sahl El Gallaba Plain, where numerous samples possess a depleted isotopic signature, indicating recharge from the deep NSAS to the shallow QAS.

ACKNOWLEDGEMENTS

We would like to express my sincere gratitude to the editor for his valuable guidance and support throughout the review process. I am also deeply appreciative of the insightful comments and constructive suggestions provided by the two anonymous reviewers, which have enhanced the manuscript.

REFERENCES

[1]. S. A. Araffa, S. Bedair, Application of Land Magnetic and Geoelectrical Techniques for Delineating Groundwater Aquifer: Case Study in East Oweinat, Western Desert, Egypt. Nat.l Res. Res., 30 (2021), 4219–4233. https://doi.org/10.1007/s11053-021-09937-y

[2]. H. R. Burger, A. F. Sheehan, and C. H. Jones, Introduction to Applied Geophysics: Exploring the Shallow Subsurface. Cambridge: Cambridge University Press, 2023.

[3]. J. Milsom, Field Geophysics, 3rd ed. Wiley, 2003.

[4]. C.R. Fitts, Groundwater Science, Elsevier Scientific Publishers, Amsterdam, 2002.

[5]. R.A. Freeze and J.A. Cherry, Groundwater, Prentice-Hall Inc., Englewood Cliffs, vol.7632, 1979, p. 604.

[6]. J. Tóth, "A theoretical analysis of groundwater flow in small drainage basins," Journal of Geophysical Research, vol. 68, no. 16, 1963, pp. 4795-4812. https://doi.org/10.1029/JZ068i016p04795

[7]. V. Bense, T. Gleeson, S. Loveless, O. Bour, and J. Scibek, "Fault zone hydrogeology," Earth-Science Reviews, vol.127, 2013, pp. 171-192. https://doi.org/10.1016/j.earscirev.2013.09.008

[8]. T. Gleeson and A. H. Manning, "Regional groundwater flow in mountainous terrain: Three-dimensional simulations of topographic and hydrogeologic controls," Water Resources Research, vol. 44, 2008. https://doi.org/10.1029/2008wr006848

[9]. V. L. McGuire, Water-level and recoverable water in storage changes, High Plains aquifer, predevelopment to 2015 and 2013–15: U.S. Geological Survey Scientific Investigations Report2017–5040, 14 p., https://doi.org/10.3133/sir20175040.

[10]. Conoco Coral (1987) Geological Map of Egypt, Cairo, Egypt, NG 36 NW Asyut sheet, Scale 1:500,000.

[11]. F. Hendriks, J. Luger, 2. Bovitz, and H. Kallenbach, "Evolution of the depositional environments of SE Egypt during the Cretaceous and lower Tertiary,"Berliner Geowissenschaftliche Abhandlungen, vol. 75(A), 1987, pp. 49-82.

[12]. M. Hermina, "The surroundings of Kharga, Dakhla and Farafra oases," in The Geology of Egypt, 1990, pp. 259–292. https://doi.org/10.1201/9780203736678-14

[13]. M. H. El-Azabi and S. Farouk, "High-resolution sequence stratigraphy of the Maastrichtian- Ypresian succession along the eastern scarp face of Kharga Oasis, southern Western Desert, Egypt," Sedimentology, vol. 58, no. 3, 2011, pp. 579–617. https://doi.org/10.1111/j.1365-3091.2010.01175.x

[14]. K. A. K. Ouda, "The Nubia Sandstone (Nubia Group), Western Desert, Egypt: An Overview," International Journal of Trend in Scientific Research and Development, vol. 5, no. 3, 2021. Available: www.ijtsrd.com

[15]. R. Said, (1981). The GEOLOGICAL EVOLUTION of the RIVER NILE. Springer, New York. https://doi.org/10.1007/978-1-4612-5841-4

[16]. U. Thorweihe, "Nubian Aquifer system," in The Geology of Egypt, 1990, pp. 601-611. https://doi.org/10.1201/9780203736678-28

[17]. H.I. Abdel-Shafy and A.H. Kamel, "Groundwater in Egypt Issue: Resources, Location, Amount, Contamination, Protection, Renewal, Future Overview," Egyptian Journal of Chemistry, vol. 59, no. 3, 2016, pp. 321–362. https://doi.org/10.21608/EJCHEM.2016.1085

[18]. M.R. El Tahlawi, A.A. Farrag, and S.S. Ahmed, "Groundwater of Egypt: An environmental overview" Environmental Geology, vol. 55, no. 3, 2008, pp. 639–652. https://doi.org/10.1007/s00254-007-1014-1

[19]. Egyptian Geological Survey and Minning Authority (EGSMA) (1981). GEOLOGICAL MAP OF EGYPT, scale 1: 2,000,000.

[20]. Geosoft Inc. (2015). Oasis montaj (Version 8.4) [Computer software].

[21]. V. Baranov, "A new method for interpretation of aeromagnetic maps; pseudo-gravimetric anomalies" Geophysics, vol. 22, no. 2, pp. 359–382. https://doi.org/10.1190/1.1438369

[22]. W. M. Telford, L. P. Geldart, and R. E. Sheriff, Applied Geophysics, 1990. https://doi.org/10.1017/CBO9781139167932